Chemical Papers (2021) 75:2087–2103
https://doi.org/10.1007/s11696-020-01469-8

ORIGINAL PAPER

Effect of reduction and reaction conditions on the catalytic performance of Co–Ni/Al_2O_3 catalyst in CO hydrogenation: modeling of surface reaction rate

Ali Akbar Mirzaei[1] · Mohammad Farahi[1] · Maryam Akbari[1]

Received: 30 July 2020 / Accepted: 9 December 2020 / Published online: 5 January 2021

Abstract
The effect of reduction and reaction conditions on catalytic performance and surface reaction rate of Fischer–Tropsch synthesis over Co–Ni/Al_2O_3 catalyst was studied in a stainless steel fixed-bed micro-reactor. Experiments were done over a collection of different reduction and reaction conditions, including reduction temperature (250–450 °C), reduction time (2–10 h), reducing agent (H_2, CO and mixing of H_2 and CO), reaction temperature (150–240 °C), H_2/CO (1–4) and reaction pressure (1–5 bar). In particular, the modeling of the effect of reduction and reaction conditions on the CO consumption rate was studied by response surface methodology. The surface reaction rates are important in scale-up of a FT reactor, industrial design, and simulation. The accuracy of created models was proved by ANOVA and diagnostic plots. According to the obtained quadratic polynomial equations, the order of parameters influence on CO consumption rate response was argued. Regard to results obtained, the main effective reduction and reaction parameters on CO consumption rate were reducing agent and reaction pressure, respectively. Furthermore, the precursor and catalysts before and after the test were characterized by XRD and SEM.

Keywords Fischer–Tropsch synthesis · Cobalt–nickel catalyst · Surface reaction rate · Modeling · Response surface methodology

Introduction

Fischer–Tropsch Synthesis (FTS), a pseudo-polymerization catalytic synthesis, converts natural gas, coal, and biomass-derived syngas (the combination of carbon monoxide and hydrogen) to a wide range of hydrocarbon products: light olefins to liquid long-chain hydrocarbons (fuels). Unlike petroleum-derived ones, fuels from FTS are known as clean fuels, because they do not have any sulfur, nitrogen, chlorine compounds (i.e., COS, H_2S, NH_3, HCN, HCl), and consequently, environmental pollution (Rahmati et al. 2018; Akbari et al. 2019; Yaghoobpour et al. 2020). Decrease of oil resources (which leads to a rise in crude oil price), along with the increase in the discovery of shale gas and gas fields, magnet the attention of industry and academia to the Fischer–Tropsch reaction. The main representative FTS reactions for hydrocarbon production are as below:

$$Alkane\ production: (2n+1)H_2(g) + nCO(g) \rightarrow C_nH_{2n+2} + nH_2O \quad (1)$$

$$Alkene\ production: (2n)H_2(g) + nCO(g) \rightarrow C_nH_{2n} + nH_2O \quad (2)$$

$$Water-gas\ shift\ reaction: H_2O + CO \rightarrow CO_2 + H_2 \quad (3)$$

The chemical reaction of FTS takes place over the active sites of a FT catalyst. Hitherto, only four transitional metals of cobalt, iron, nickel, and ruthenium are considered active for FTS. Despite the high activity of ruthenium in FTS, the low abundance and very high price lead to its un-usability in the industry (Martinelli et al. 2020). Nickel has a lower price and high activity in conversion of syngas, but because of high hydrogenation capability (Shafer et al. 2019),

✉ Maryam Akbari
m.akbary@pgs.usb.ac.ir; maryam.akbary1366@gmail.com

[1] Department of Chemistry, Faculty of Sciences, University of Sistan and Baluchestan, P.O. Box 98135-674, Zahedan, Iran

short-chained hydrocarbons, especially CH_4, is the dominant product. Therefore, only cobalt and iron have conventionally been considered for industrial usage. Although cobalt has higher price rather than iron, there are unique properties for it: higher activity in FTS at lower reaction temperature, the lower water–gas shift (WGS) reaction activity, better resistance to deactivation due to byproduct water formation, being suitable for high H_2/CO syngas conversion (Rahmati et al. 2018; Jahangiri et al. 2014; Tsakoumis et al. 2010; Liu et al. 2020a). One manner of the modification of catalytic behavior is the usage of two metals components. This technique leads to the perturbation of pure electronic structures, resulting in new exposing orbitals (differ from pure atomic orbitals) at the active site surface (Ponec 2001). Liu and co-workers used Ni–Co catalysts for the production of both liquid fuels and methane from syngas (Liu et al. 2020b). They concluded that the synergistic interaction between Co and Ni, has a vital role in the improvement of catalytic activity and total yield of liquid fuels and methane. Also, they stated that the composition of the main products could be adjusted by the Ni/Co ratio and the operating conditions. Helden and co-workers, through a DFT-based computations, revealed that Co–Ni bimetallic catalyst could be an alternative catalyst for FTS (Helden et al. 2020). Also, they experimentally demonstrated that Co–Ni alloys, with a nickel content of up to 25%, perform similar to pure Co in FTS. Moreover, this bimetallic catalyst will be cheaper than pure Co one. Martinelli and co-workers verified that the addition of Ni enhances the cobalt reducibility (Martinelli et al. 2020). Also, they concluded that the catalyst with the Co/Ni ratio of 75/25 demonstrated better performance rather than the pure catalyst in FTS. Arsalanfar and co-workers evaluated the effect of calcination and process conditions on FT catalytic performance of the Co–Ni/Al_2O_3 catalyst prepared by the sol–gel method (Arsalanfar et al. 2020).

Before beginning the FTS, there is an important step: the reduction of the prepared catalyst. The catalyst after calcination step contains metal oxides, which are inactive in FTS. The active phases of Co and Ni catalysts are the metallic ones (Akbari et al. 2019; Azizi et al. 2014). During the reduction step, the inactive species experience a complex phase transformation, which results in the formation of the active catalyst (Nisa et al. 2020). Therefore, the reduction conditions have a crucial effect on catalytic performance. After the reduction step, the Fischer–Tropsch operating conditions are applied. At these steps, based on the reaction mechanism, hydrocarbon formation happens (Moazami et al. 2017). It is well known that the reaction conditions, through influence on relative rates of different elementary reactions and composition of the active surface, play an important role in the surface reaction rates and catalytic performance (Schulz 2013; Niu et al. 2020). Many researchers have focused on the impact of the FTS process conditions (Niu et al. 2020; Abbasi et al. 2019; Arsalanfar et al. 2012; Feyzi et al. 2012; Zare et al. 2013), but there are few studies have been provided statistical models presented the importance of these parameters and characterized the main effective factor. Statistical modeling is a useful and valuable methodology for the development of catalyst performance description, especially for multi-factor experiments (Atashi et al. 2015; Akbari et al. 2018).

In the current study, we studied the impact of reduction and reaction conditions on the FT catalytic performance (catalytic activity and product selectivities) of Co–Ni/Al_2O_3 prepared by fusion method. The studied parameters consist of reduction temperature (250–450 °C), reduction time (2–10 h), reducing agent (H_2, CO, and H_2 + CO), and a wide range of process conditions (reaction temperature of 150–240 °C, H_2/CO molar ratio of 1–4 and pressure of 1–5 bar). To evaluate the catalytic performance, a lab-scale fixed-bed reactor was used. Since the surface reaction rates are significant in scale-up of a FT reactor, industrial design, and simulation, the modeling of the effect of reduction and reaction conditions on surface reaction rate using response surface methodology (RSM), a modern tool for modeling, was done. To the best of our knowledge, there is no study about the modeling of the effect of reduction and reaction parameters on CO consumption rate. In the following, based on the equations obtained and coefficients of parameters, the order of parameters influences on studied response discussed.

Experimental

Preparation of Co–Ni/Al_2O_3 catalyst

In the current work, alumina supported Co–Ni catalyst was prepared by the fusion method. For this purpose, the necessary amounts of cobalt (II) nitrate ($Co(NO_3)_2.6H_2O$, 99%, Merck), and nickel (II) nitrate ($Ni(NO_3)_2.6H_2O$, 97%, Merck) were completely eroded and mixed. Then, the alumina (Al_2O_3, Merck) was added to the previous combination and again mixed. The required amount of materials were in accordance to final nominal composition of 80 wt% Co-20 wt% Ni/3 wt% Al_2O_3. The powder was heated at 120 °C for 16 h. After the cooling and grounding the melted combination, the obtained powder was transferred to a crucible, heated in an electric furnace at 1500 °C for 7 h, and cooled naturally to room temperature in the furnace. The final catalyst was obtained since the crushing of the sample obtained after the furnace step.

Catalyst characterization

X-ray diffraction (XRD) patterns of the catalysts at different steps were obtained with a D5000 Advance diffractometer (Bruker AXS, Germany) operated at 25 mA and 35 kV, with Cu Kα radiation source ($\lambda = 0.15406$ nm). Scans were derived with a 2θ step size of 10° and a step time of 1 s.

Scanning electron microscopy (SEM) was performed on a Cambridge S-360 instrument (England) with a 20 kV beam.

Reactor system and catalytic evaluation

The FTS tests were carried out in a lab-scale fixed-bed stainless steel reactor with an inner diameter of 20 mm and a total length of 100 cm. A representation of the used fixed-bed reactor system is displayed in Fig. 1 (Mirzaei et al. 2015). In each run, 1 g catalyst was diluted with asbestos (due to the exothermic nature of FTS) and positioned among the inert quartz glass beads. The reactor was surrounded by a tubular furnace (Atbin, Model ATU 150–15). To improve the temperature uniformity of the catalyst bed, an alumina jacket was employed between the reactor and the internal furnace wall. The catalyst was in situ activated using the mixture of H_2 (> 99.99%) and N_2 (> 99.99%) gases ($H_2/N_2 = 1/1$ and the flow rate of each gas was 30 ml. min^{-1}) or CO (99%) and N_2 ($CO/N_2 = 30/30$ (v/v)) mixture, or H_2-CO-N_2 ($H_2/CO/N_2 = 15/15/30$ (v/v/v)) mixture, at different temperatures (250–450 °C) and times (2–10 h) under atmospheric pressure. It is worth mentioning that in the evaluation of reduction conditions, each of the experiments was done with a new catalyst. For example, 1 gr catalyst was placed in the reactor, and reduced under H_2 atmosphere, at a specific reduction temperature and time. After the end of the reduction step, the catalyst was taken to the intended reactor condition. In the step of evaluation of reaction conditions, 1 gr catalyst was located in the reactor. Then, the experiments with similar reactor conditions except for temperature (for example), were performed. After each temperature variation, it gave enough time to ensure steady state behavior (this time was higher at higher pressures). It is worth noting that before the start of the main work, a pre-test were done, to ensure the catalyst stability, in which the studied catalyst demonstrated good stability during 72 h. Also, in each reactor condition, three consecutive analyzes were performed to ensure the stability of the catalyst behavior.

The flow rate of the gases was automatically adjusted by mass flow controllers (Brooks, USA; model 5850E), which was calibrated by soap bubble flow meter. After the reduction step, the reactor was cooled down to reaction

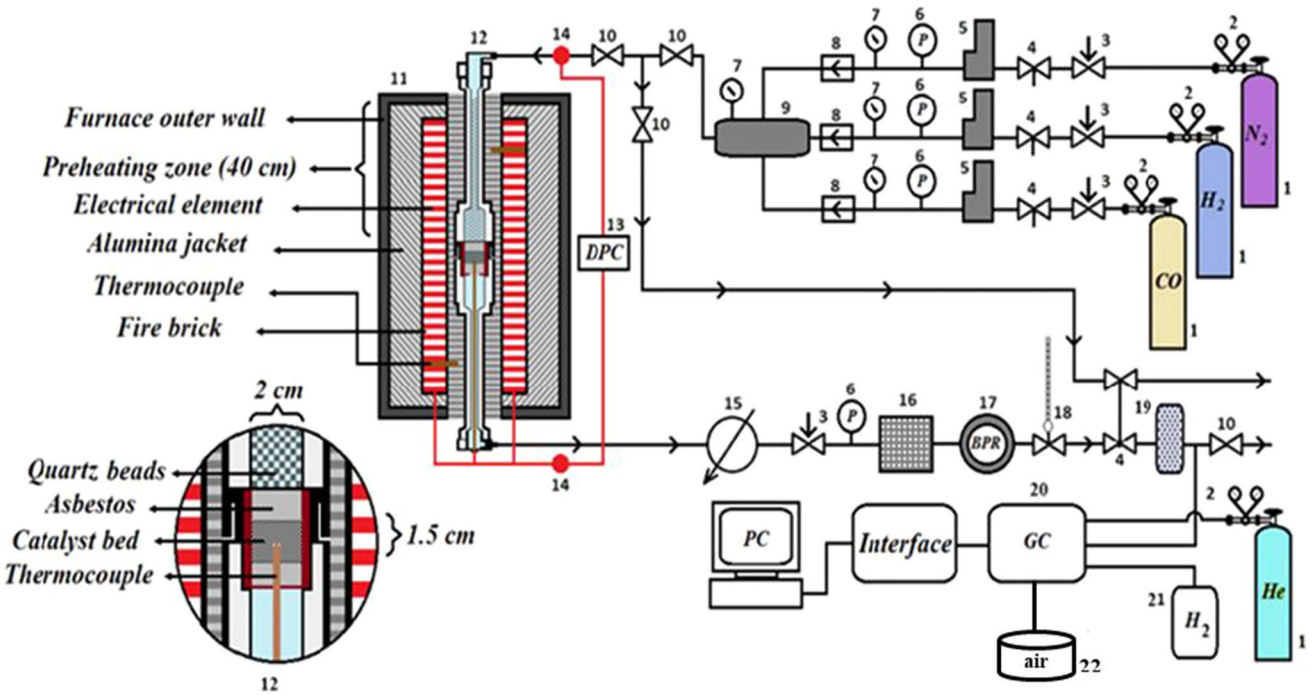

Fig. 1 A schematic illustration of experimental set up: 1- gas cylinders, 2- pressure regulators, 3- needle valves, 4- ball valves, 5- mass flow controllers (MFC), 6- digital pressure controllers, 7- pressure gauges, 8- non return valves, 9- mixing chamber, 10- valves, 11- tubular furnace, 12- tubular reactor and catalyst bed, 13- temperature indicators (digital program controller), 14- resistance temperature detector (RTD), 15- condenser, 16- trap air, 17- BPR (back pressure regulator), 18- flow meter, 19- silica gel column, 20- gas chromatograph (GC), 21-hydrogen generator, 22- air compressor

temperature (different reaction temperatures between 150–240 °C). Then, the syngas (H_2-CO-15%N_2) with different H_2/CO (v/v) ratios (1–4) was entered into the reactor. The pressure of the system was regulated at different pressures (1–5 bars) using the back pressure regulator.

The analysis of reactant gases and gained products were performed using an online gas chromatograph (Thermo ONIX UNICAM PROGC +) with two kinds of detectors: thermal conductivity detector (TCD) and flame ionization detector (FID). TCD with two series packed column (Hayesep QS (3 m, 1/8") and molecular Sieve (2 m, 1/8")) and He as the carrier gas was used for the analysis of reactant gases, and FID with a capillary column (30 m, 0.53 mm ID) was utilized for the study of hydrocarbons. The GC calibration was performed using pure compounds and several calibration mixtures.

CO conversion and hydrocarbon selectivities were calculated using the succeeding formulas:

$$CO\ conversion\,(\%) = \frac{n_{CO}^{in} - n_{CO}^{out}}{n_{CO}^{in}} \times 100 \tag{4}$$

$$Selectivity\ of\ hydrocarbon\ i\,(\%) = \frac{n_i N_i}{n_{CO}^{in} - n_{CO}^{out}} \times 100, \tag{5}$$

where n_{CO}^{in} and n_{CO}^{out} symbolize the moles of CO at the inlet and outlet, respectively, n_i is the carbon number of hydrocarbon i, and N_i is moles of hydrocarbon i. In all testes, CO_2 was undetectable; then only hydrocarbons were contained in selectivity calculations. In each test, the relative deviation of carbon balance was lower than 5%.

To evaluate the effect of reduction and reaction conditions on surface reaction rate, the following formulas were used:

$$-r_{CO} = \frac{X_{CO} F_{CO}^0}{W_{cat}} \tag{6}$$

and

$$F_{CO}^0 = \frac{v_0 P_{CO}}{RT} \tag{7}$$

where r_{CO} is CO consumption rate (mol.min^{-1}.g^{-1}), F_{CO}^0 is inlet molar flow of CO (mol.min^{-1}), W_{cat} is catalyst mass (g), v_0 is the volumetric flow rate of feed gas (ml/min), P_{CO} is the partial pressure of CO (bar), R is the universal gas constant (83.14 ml.bar.mol^{-1}.K^{-1}), and T is temperature (K).

Modeling method

A statistical model is a mathematical representation of the relationship between one or further independent parameters (input factors) and responses (output factors). Using the statistical model, one can describe the process and detect the main factors and the interaction between them. An appropriate method for fitting a quadratic surface and analyzing the interaction between the factors is response surface methodology (RSM) (Atashi and Rezaeian 2019).

In this study, by the use of RSM, the influence of independent factors of reduction conditions (reduction temperature, reduction time, and reducing agents) and reaction conditions (reaction temperature, H_2/CO, and reaction pressure) on CO consumption rate was assessed.

A second-order empirical model linked response to controllable input factors can be written as follows:

$$Y = b_0 + \sum_{i=1}^{n} b_i X_i + \sum_{i=1}^{n} b_{ii} X_i^2 + \sum_{i=1}^{n} \sum_{j>1}^{n} b_{ij} X_i X_j + \varepsilon \tag{8}$$

where Y is the process response, X_i and X_j are independent factors, b_0 is the constant coefficient, b_i is the linear coefficient of X_i, b_{ii} is the quadratic coefficient of X_i, b_{ij} is the interaction coefficient between X_i and X_j and ε is the random error.

R^2 and R^2_{adj} are used for the evaluation of the consent degree of the polynomial equation provided in Eq. (8). R^2 is the multiple correlation coefficient which measures the amount of variation about the mean specified by the model and is computed as below:

$$R^2 = 1 - \frac{SS_{residual}}{SS_{\mathrm{mod}\ el} + SS_{residual}} \tag{9}$$

R^2_{adj} is a measure of the amount of variation about the mean explained by the model and adjusted for the number of terms in the model. R^2_{adj} is calculated as below:

$$R^2_{adj} = 1 - \frac{SS_{residual}/DF_{residual}}{(SS_{\mathrm{mod}\ el} + SS_{residual})/(DF_{\mathrm{mod}\ el} + DF_{residual})} \tag{10}$$

where SS is the sum of squares, and DF is the degree of freedom. The high value of R^2 can be gotten by eliminating or adding the terms. But the R^2_{adj} decreases as the number of terms in the model increases if those additional terms do not improve value to the model. Therefore, R^2_{adj} is favored as a more unbiased valuation.

Adequate precision is a signal-to-noise ratio, and its desired value is 4 or more. In other words, ratios more than 4 points to adequate model discrimination. This criterion could be computed as below:

$$Adequate\ precision = \frac{\max(\hat{y}) - \min(\hat{y})}{\sqrt{\overline{V}(\hat{y})}} \tag{11}$$

$$\overline{V}(\hat{y}) = \frac{1}{n}\sum_{i=1}^{n} V(\hat{y}) = \frac{P\sigma^2}{n}, \quad (12)$$

where n is the number of experiments, P is the number of model parameters, $\hat{y}$ is the predicted response, and σ^2 is the residual mean square.

Further criteria to evaluate the statistical significance are p and F values. The individual terms in the model have an important influence on the response if the Prob > F value is very small (less than 0.05). The reverse pattern is true for F value.

Results and discussion

In the current work, the modeling of the effect of reduction and reaction conditions on the CO consumption rate of Co–Ni/Al_2O_3 catalyst in FTS, which has not been studied so far, has been considered. Here, the input factors contain reduction temperature, reduction time, reducing agent, reaction temperature, reaction pressure, and H_2/CO ratio. The experimental data are provided in Tables 1 and 2. Before the discussion on CO consumption rate models, graphs, diagnostics plots, and detection of the prominence of factors, the

Table 1 Experimental results for the catalytic performance of Co–Ni/Al_2O_3 catalyst under different reduction conditions (reaction temperature is 170 °C, H_2/CO = 1/1, and reaction pressure is 1 bar)

Run	Reduction temperature (°C)	Reduction time (h)	Reducing agent	CO (%)	CH_4	C_2H_6	C_2H_4	C_3H_8	C_3H_6
1	250.00	2.00	H_2	20	60	8	6	17	9
2	300.00	2.00	H_2	25	61	10	5	13	11
3	350.00	2.00	H_2	27	62	13	4	12	9
4	400.00	2.00	H_2	34	58	11	7	9	15
5	450.00	2.00	H_2	32	63	9	5	15	8
6	400.00	4.00	H_2	28	60	12	4	14	10
7	400.00	6.00	H_2	30	61	9	6	16	8
8	400.00	8.00	H_2	25	63	14	5	12	6
9	400.00	10.00	H_2	22	65	13	3	15	4
10	400.00	2.00	CO	40	65	13	5	11	6
11	400.00	2.00	H_2 + CO	52	67	14	3	12	4

Table 2 Experimental results for the catalytic performance of Co–Ni/Al_2O_3 catalyst under different reaction conditions

Run	T (°C)	H_2/CO	P (bar)	CO (%)	CH_4	C_2H_6	C_2H_4	C_3H_8	C_3H_6
1	150.00	2.00	1.00	23	52	15	5	13	15
2	160.00	2.00	1.00	27	55	13	6	12	14
3	170.00	2.00	1.00	34	58	11	7	9	15
4	180.00	2.00	1.00	40	49	10	15	7	19
5	190.00	2.00	1.00	42	63	12	6	9	10
6	200.00	2.00	1.00	57	89	6	0	5	0
7	210.00	2.00	1.00	66	95	3	0	2	0
8	220.00	2.00	1.00	74	100	0	0	0	0
9	230.00	2.00	1.00	83	100	0	0	0	0
10	240.00	2.00	1.00	92	100	0	0	0	0
11	180.00	1.00	1.00	34	58	11	7	9	15
12	180.00	3.00	1.00	41	57	15	6	10	12
13	180.00	4.00	1.00	42	62	16	5	9	8
14	180.00	2.00	2.00	48	57	17	8	10	8
15	180.00	2.00	3.00	55	64	14	6	7	9
16	180.00	2.00	4.00	63	70	12	5	6	7
17	180.00	2.00	5.00	70	77	11	3	4	5

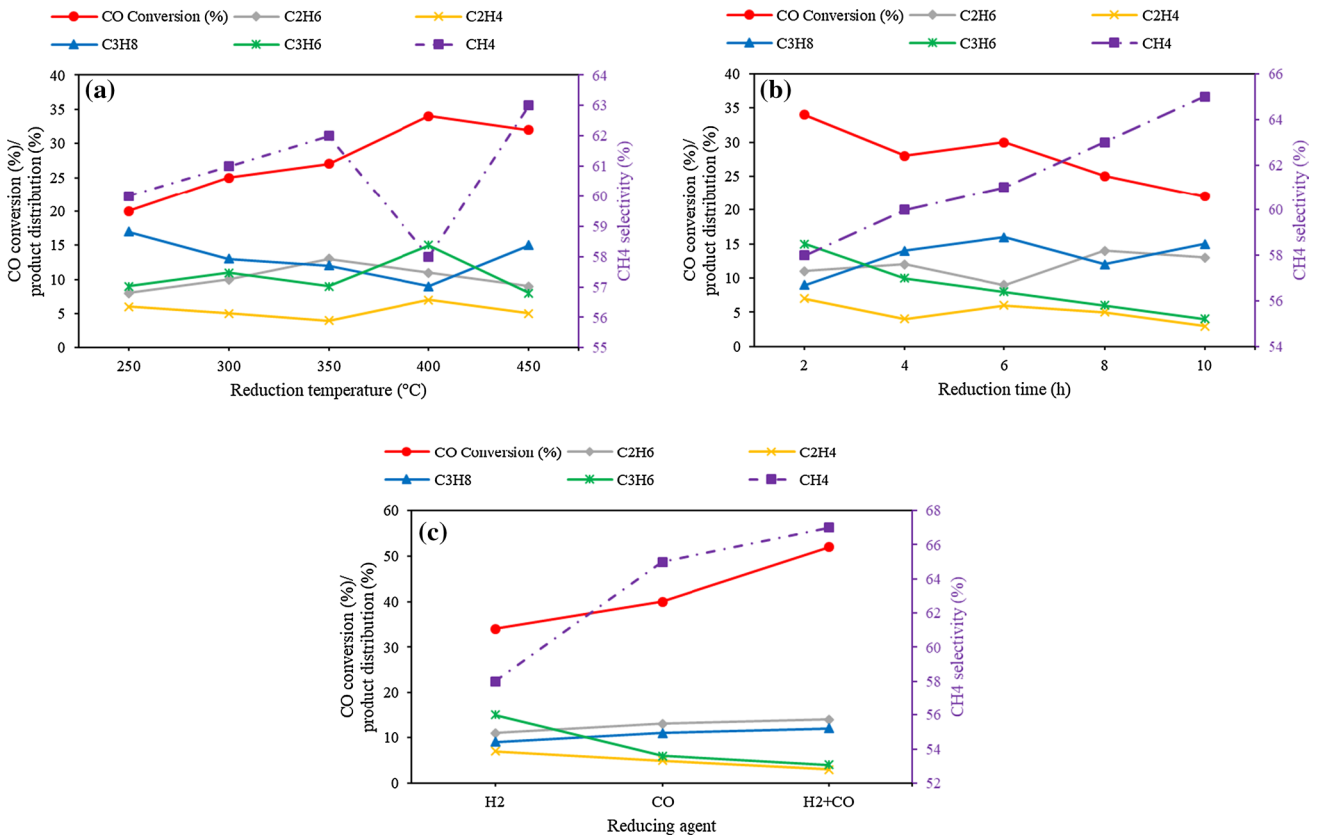

Fig. 2 Effect of reduction temperature (**a**), reduction time (**b**), and reducing agent (**c**) on catalytic activity and product selectivities of Co–Ni/Al_2O_3 catalyst

effect of studied parameters on catalytic activity and product selectivities has been argued. Finally, some of the characterization analysis of catalyst has been studied. Response surface methodology, ANOVA, regressions, and modeling of parameters were performed through design expert 7.0.0 software.

Effect of reduction conditions on the catalytic performance of Co–Ni/Al_2O_3catalyst

The effect of reduction conditions on catalytic activity and product selectivities of the Co–Ni/Al_2O_3 catalyst is illustrated in Fig. 2. At this step, the reaction temperature is 170 °C, H_2/CO molar ratio is 1/1 and, reaction pressure is 1 bar. It is worth mentioning that the FTS has been considered as a proposed course for the production of light olefins from non-oil sources (addition to the production of fuels). Light olefins (ethylene and propylene) have a vital role in the chemical industries such as construction manufacturing, packaging, etc. (Akbari et al. 2019; Torres Galvis and Jong 2013; Weissman and Anderson 2014). Therefore, experimental conditions chosen for this set of experiments are in line with the production of light olefins and, therefore, are different from typical representative reaction condition for FTS on cobalt or Ni–Co catalyst (which their goal is the production of fuels and high molecular weight hydrocarbons) (Torres Galvis and Jong 2013; Mirzaei et al. 2007; Copperthwaite et al. 1987).

As can be seen in Fig. 2a, with an increase in reduction temperature (from 250 to 450 °C), the CO conversion and CH_4 selectivity passed from a maximum and clear minimum at 400 °C, respectively. Also, at reduction temperature of 400 °C, the C_3H_6 selectivity is more than C_3H_8 one.

The effect of reduction time on Co–Ni/Al_2O_3 catalytic activity and product selectivities is illustrated in Fig. 2b. The experimental results revealed that with an increase in reduction time (from 2 to 10 h), the CH_4 selectivity increased, while CO conversion, C_3H_6, and C_2H_4 selectivities demonstrated overall dropping trends.

The effect of reducing agents on Co–Ni/Al_2O_3 catalytic activity and product selectivities is shown in Fig. 2c. The empirical data revealed that reduction under H_2 and CO mixture gas atmosphere led to higher CO conversion than other studied atmospheres, but high CH_4 selectivity of this reducing atmosphere led to the unsuitability of this atmosphere for the production of light olefins. While reduction

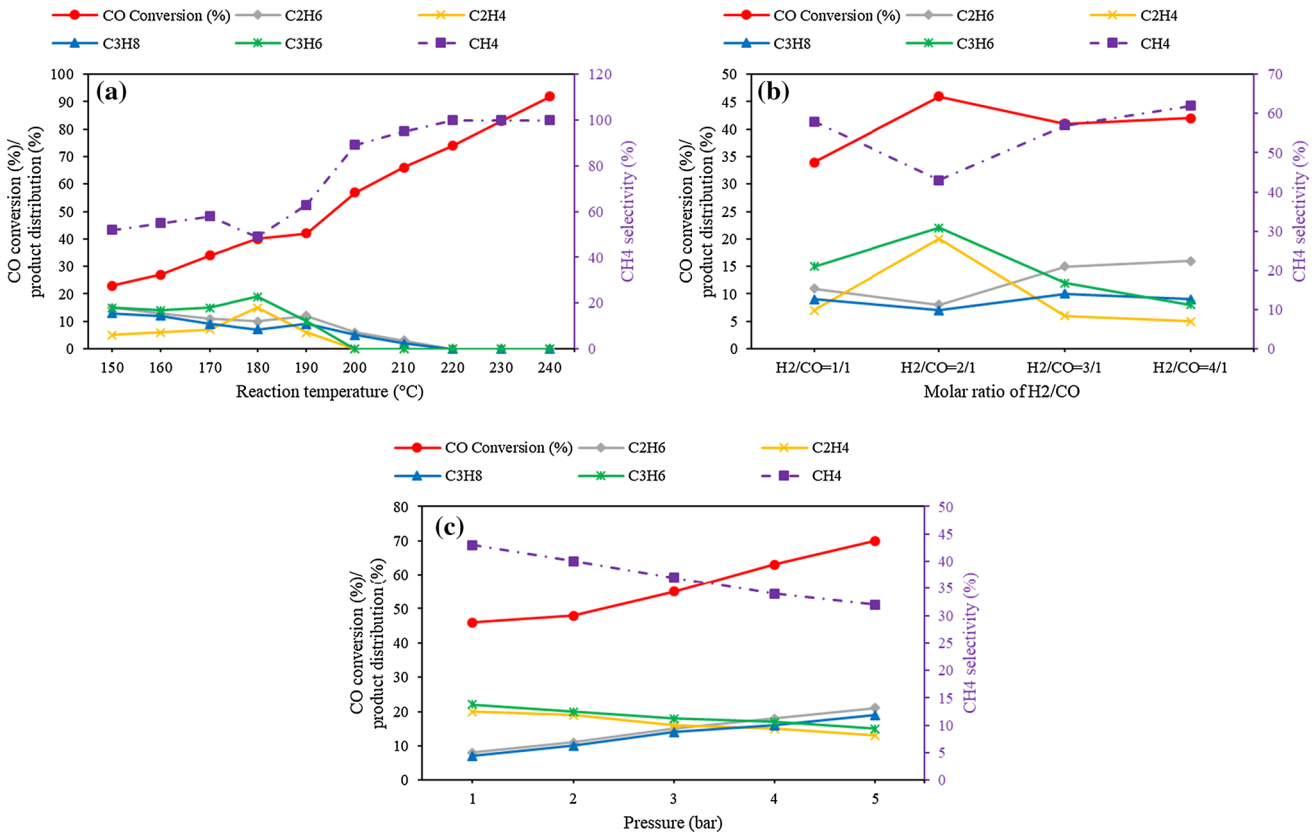

Fig. 3 Effect of reaction temperature (**a**), H_2/CO (**b**), and pressure (**c**) on catalytic activity and product selectivities of Co–Ni/Al_2O_3 catalyst

under H_2 atmosphere resulted in lower methane selectivity and higher propylene selectivity rather than other considered atmospheres.

Effect of reaction conditions on the catalytic performance of the Co–Ni/Al_2O_3 catalyst

The effect of reaction conditions on catalytic activity and product selectivities of Co–Ni/Al_2O_3 catalyst is illustrated in Fig. 3. As can be observed in Fig. 3a, an increase in reaction temperature led to an increase in CO conversion and methane selectivity. At a temperature of 200 °C, the only product manufactured is methane, and the CO conversion is 100%, which makes this catalyst a suitable candidate for CO methanation reaction at low temperature. For FTS, an exothermic reaction, it is well known that a rise of temperature leads to a shift towards products with a lower carbon (Laan and Beenackers 1999). Empirical data illustrated that increase of reaction temperature up to 180 °C, led to increased selectivity of olefin formations, which could be explained by increment the rate of dehydrogenation reaction with an increase of reaction temperature (Sethuraman et al. 2001).

The effect of H_2/CO molar ration on Co–Ni/Al_2O_3 catalytic activity and product selectivities is illustrated in Fig. 3b. The collected results demonstrated that with an increase in H_2/CO molar ratio from 1/1 to 4/1, the CO conversion showed an enhanced trend and high paraffinic content was prominent, which could be related to higher termination rate into paraffins (Zarrin et al. 2009).

The effect of reaction pressure on Co–Ni/Al_2O_3 catalytic activity and product selectivities is presented in Fig. 3c. As can be seen, an increase in reaction pressure resulted in the improvement of CO conversion and depletion of methane selectivity. The reduced methane selectivity could be related to more contribution of individual CH_2 units in chain growth, with an increase in total pressure (Sari et al. 2009; Fazlollahi et al. 2012). Also, as it is clarified in Fig. 3(c), with an increase in the pressure, the light olefins selectivity reduced. This behavior could be interpreted by considering

Table 3 Empirical data of the effect of reduction conditions on $Co–Ni/Al_2O_3$ catalytic activity

Run	A Reduction temperature (°C)	B Reduction time (h)	C Reducing agent	CO (%)	r_{CO} (mmol/min.g) (experimental)	r_{CO} (mmol/min.g) (predicted)
1	250.00	2.00	H_2	20	2.44E−01	0.24
2	300.00	2.00	H_2	25	3.05E−01	0.30
3	350.00	2.00	H_2	27	3.29E−01	0.35
4	400.00	2.00	H_2	34	4.14E−01	0.38
5	450.00	2.00	H_2	32	3.90E−01	0.40
6	400.00	4.00	H_2	28	3.41E−01	0.37
7	400.00	6.00	H_2	30	3.66E−01	0.34
8	400.00	8.00	H_2	25	3.05E−01	0.31
9	400.00	10.00	H_2	22	2.68E−01	0.27
10	400.00	2.00	CO	40	4.87E−01	0.49
11	400.00	2.00	H_2+CO	52	6.34E−01	0.63

Table 4 Experimental data of the effect of reaction conditions on $Co–Ni/Al_2O_3$ catalytic activity

Run	A T (°C)	B H_2/CO	C P (bar)	CO (%)	r_{CO} (mmol/min.g) (experimental)	r_{CO} (mmol/min.g) (predicted)
1	150.00	2.00	1.00	23	1.85E−01	0.18
2	160.00	2.00	1.00	27	2.17E−01	0.22
3	170.00	2.00	1.00	34	2.73E−01	0.27
4	180.00	2.00	1.00	40	3.22E−01	0.32
5	190.00	2.00	1.00	42	3.38E−01	0.38
6	200.00	2.00	1.00	57	4.58E−01	0.44
7	210.00	2.00	1.00	66	5.31E−01	0.51
8	220.00	2.00	1.00	74	5.95E−01	0.59
9	230.00	2.00	1.00	83	6.67E−01	0.67
10	240.00	2.00	1.00	92	7.40E−01	0.75
11	180.00	1.00	1.00	34	4.14E−01	0.41
12	180.00	3.00	1.00	41	2.50E−01	0.25
13	180.00	4.00	1.00	42	2.05E−01	0.20
14	180.00	2.00	2.00	48	7.72E−01	0.77
15	180.00	2.00	3.00	55	1.33E+00	1.34
16	180.00	2.00	4.00	63	2.03E+00	2.02
17	180.00	2.00	5.00	70	2.81E+00	2.82

the olefins reactivity (Sarkari et al. 2014). Therefore, high pressure was favorable for hydrogenation reaction and formation of paraffinic products.

Modeling of CO consumption rate

Using collected experimental data and Eqs. (6) and (7), the CO consumption rate for each test was calculated. Modeling and evaluation of the significance of individual/binary influences of reduction and reaction parameters were performed by RSM. If the fitted model gotten by the least square regression has a satisfactory approximation of empirical results, it can be implemented to analyze the real system. The results demonstrated satisfactory appropriateness between empirical data and the achieved model (Tables 3 and 4).

ANOVA for response surface reduced quadratic models

The final quadratic equations for the CO consumption rate in terms of actual factors (reduction and reaction parameters) were gotten as follows:

For reducing agent of H_2:

$$r_{CO} = -0.27362 + (2.81 \times 10^{-3} \times \textit{reduction temperature}) - (9.01 \times 10^{-4} \times \textit{reduction time}) - (2.88 \times 10^{-6} \times \textit{reduction temperature}^2) - (1.09 \times 10^{-3} \times \textit{reduction time}^2) \quad (13)$$

For reducing agent of CO:

$$r_{CO} = -0.16735 + (2.81 \times 10^{-3} \times \textit{reduction temperature}) - (9.01 \times 10^{-4} \times \textit{reduction time}) - (2.88 \times 10^{-6} \times \textit{reduction temperature}^2) - (1.09 \times 10^{-3} \times \textit{reduction time}^2) \quad (14)$$

For reducing agent of H_2 + CO:

$$r_{CO} = -0.021137 + (2.81 \times 10^{-3} \times \textit{reduction temperature}) - (9.01 \times 10^{-4} \times \textit{reduction time}) - (2.88 \times 10^{-6} \times \textit{reduction temperature}^2) - (1.09 \times 10^{-3} \times \textit{reduction time}^2) \quad (15)$$

$$r_{CO} = 0.072432 - (4.14 \times 10^{-3} \times T) - \left(0.12924 \times \frac{H_2}{CO}\right) + (0.27319 \times P) + (2.69 \times 10^{-5} \times T^2) + \left(0.011833 \times \left(\frac{H_2}{CO}\right)^2\right) + (0.058495 \times P^2) \quad (16)$$

The statistical significance of the generated quadratic models was assessed via analysis of variance (ANOVA). The results of ANOVA for response surface reduced quadratic model are presented in Tables 5 and 6.

The models F values of 28.88 and 4940.99 and p values of 0.003 and < 0.0001 (less than 5%) for created models prove the significance of the models. In the case of CO consumption rate in terms of reduction conditions, A

Table 5 ANOVA for response surface reduced quadratic model for CO consumption rate (output) in terms of reduction parameters (inputs)

Source	Coefficient estimate	Sum of squares	*df*	Mean square	F value	*P* value (Prob > F)	
Model		0.12	6	0.02	28.88	0.003	Significant
A-reduction temperature	0.079	0.016	1	0.016	22.69	0.0089	
B-reduction time	− 0.056	0.011	1	0.011	15.28	0.0174	
C-reducing agent	− 0.12	0.048	2	0.024	34.84	0.0029	
A^2	− 0.029	7.35E−04	1	7.35E−04	1.06	0.3617	
B^2	− 0.017	3.31E−04	1	3.31E−04	0.48	0.5278	
R^2 = 0.9774, Adj-R^2 = 0.9436, Adeq Precision = 18.661							

Table 6 ANOVA for response surface reduced quadratic model for CO consumption rate (output) in terms of reaction parameters (inputs)

Source	Coefficient estimate	Sum of squares	*df*	Mean square	F value	*P* value (Prob > F)	
Model		8.21	6	1.37	4940.99	< 0.0001	Significant
A-T	0.29	0.34	1	0.34	1234.9	< 0.0001	
B-H_2/CO	− 0.11	0.026	1	0.026	94.71	< 0.0001	
C-P	1.25	6.16	1	6.16	22,246.57	< 0.0001	
A^2	0.055	4.05E−03	1	4.05E−03	14.63	0.0033	
B^2	0.027	8.22E−04	1	8.22E−04	2.97	0.1157	
C^2	0.23	0.065	1	0.065	234.6	< 0.0001	
R^2 = 0.9997, Adj-R^2 = 0.9995, Adeq Precision = 247.173							

(reduction temperature), B (reduction time), and C (reducing agent) are significant model terms. *P* values more than 0.1000 specify the terms are not significant. In the case of CO consumption rate in terms of reaction conditions, A (reaction temperature), B (H_2/CO), C (reaction pressure), A^2, and C^2 are significant model terms. Here, the investigation of the parameters p values and coefficient estimates discovered that the order of reduction and reaction parameters effect on CO consumption rate are as follows:

C (reducing agent) > A (reduction temperature) > B (reduction time) > A^2 > B^2.

C (reaction pressure) > A (reaction temperature) > B (H_2/CO) > C^2 > A^2 > B^2.

The high value of R^2 (0.9774 and 0.9997) and Adj-R^2 (0.9436 and 0.9995) demonstrate acceptable fitting of the empirical data and the adequacy of the created models. As mentioned before, R^2_{adj} is favored as a more unbiased valuation. Because, the high value of R^2 can be gotten by eliminating or adding the terms, but the R^2_{adj} decreases as the number of terms in the model increases if those additional terms do not improve value to the model.

The "adequate precision" of 18.661 and 247.173 (values greater than 4) shows an adequate signal. Therefore, these models can be used to navigate the design space.

As can be realized, the obtained models pass the ANOVA criterion well.

Diagnostic plots

Diagnostic plots were used to judge the statistical validation of the models. The absence of "S-shaped" curve and a normal scattering of residuals around a straight line in the normal probability plot authorize that the residuals follow a normal distribution. Such normal distribution observed in the normal probability plot of created models (Fig. 4a and b).

Predicted vs. actual graph is a graph of the predicted response values versus the actual response values. The data points in this graph should be split uniformly by the 45 degree line. A good correlation between predicted and actual values for obtained models was observed in Fig. 5a and b).

Model graphs

The perturbation (trace) graph can help to compare the effects of all the parameters in the design space. The lines signify the influence of varying each factor, whereas holding all others in a constant ratio. The perturbation (trace) plots for different obtained models are illustrated in Fig. 6a–d. Due to the qualitative nature of the reducing agent factor, a perturbation graph is drawn for each category of this factor (Fig. 6a–c). Similar behavior was observed by changing two parameters of reduction temperature (A) and time (B) at different reducing agents. In all these three graphs, the curvature slop of A and B curves are positive and negative, respectively. For example, Fig. 6a demonstrates that at the constant reducing agent of H_2 and reduction time of 6 h, with an increase in reduction temperature (from 250 to 450 °C), the CO consumption rate increased (curve A). While at the constant reducing agent of H_2 and reduction temperature of 350 °C, with an increase in reduction time, the CO consumption rate decreased (curve B).

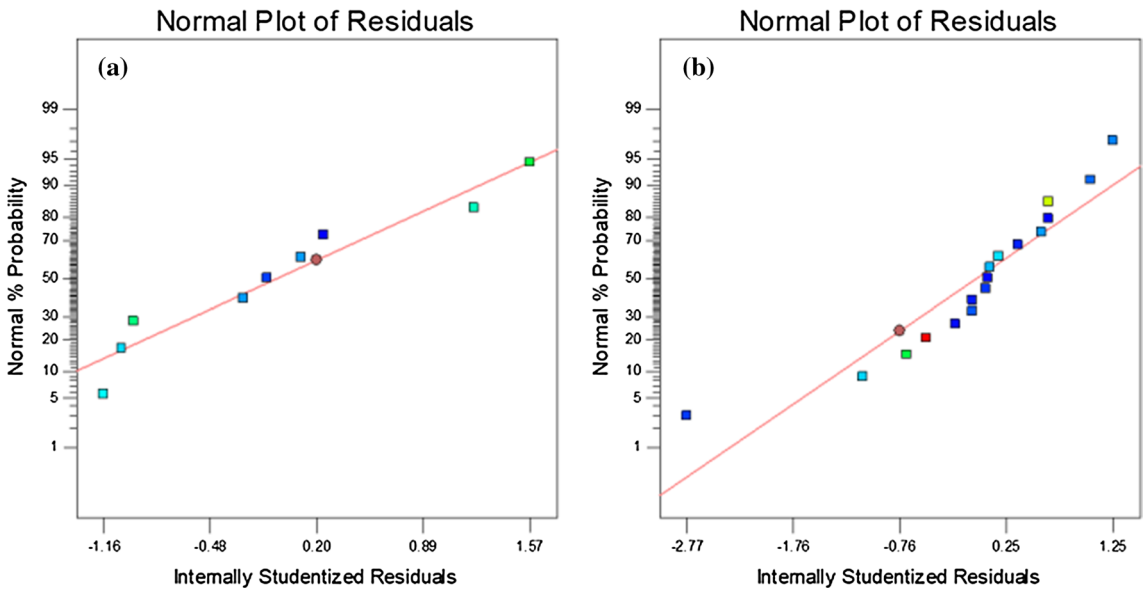

Fig. 4 Normal probability plot of residuals of CO consumption rate in terms of (**a**) reduction parameters and (**b**) reaction parameters

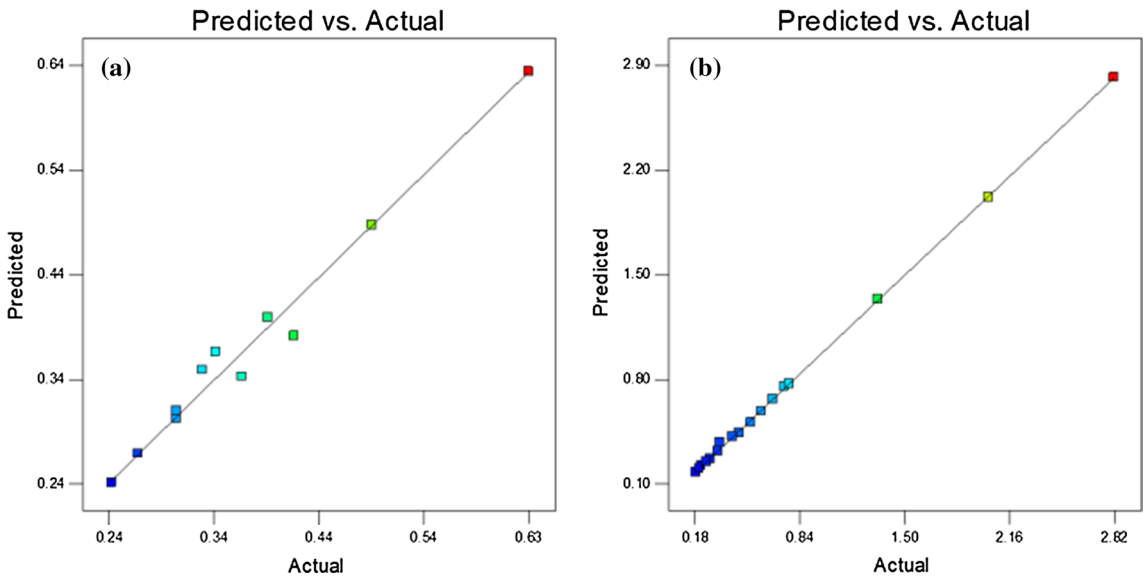

Fig. 5 Predicted versus actual plot of CO consumption rate in terms of (**a**) reduction parameters and (**b**) reaction parameters

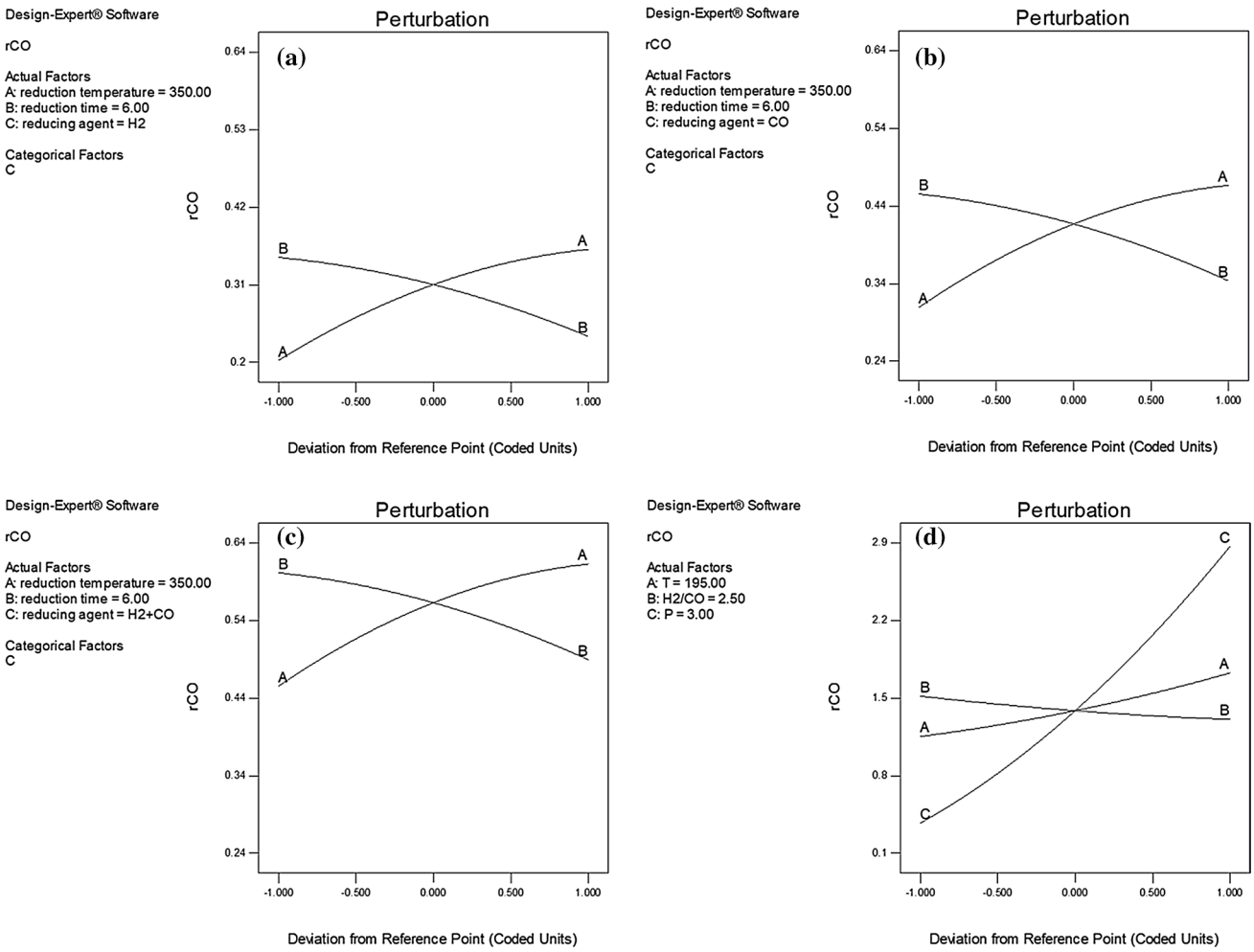

Fig. 6 Perturbation plot for CO consumption rate in terms of reduction conditions at the constant reducing agent of (**a**) H_2, (**b**) CO, (**c**) H_2+CO, and (**d**) reaction conditions

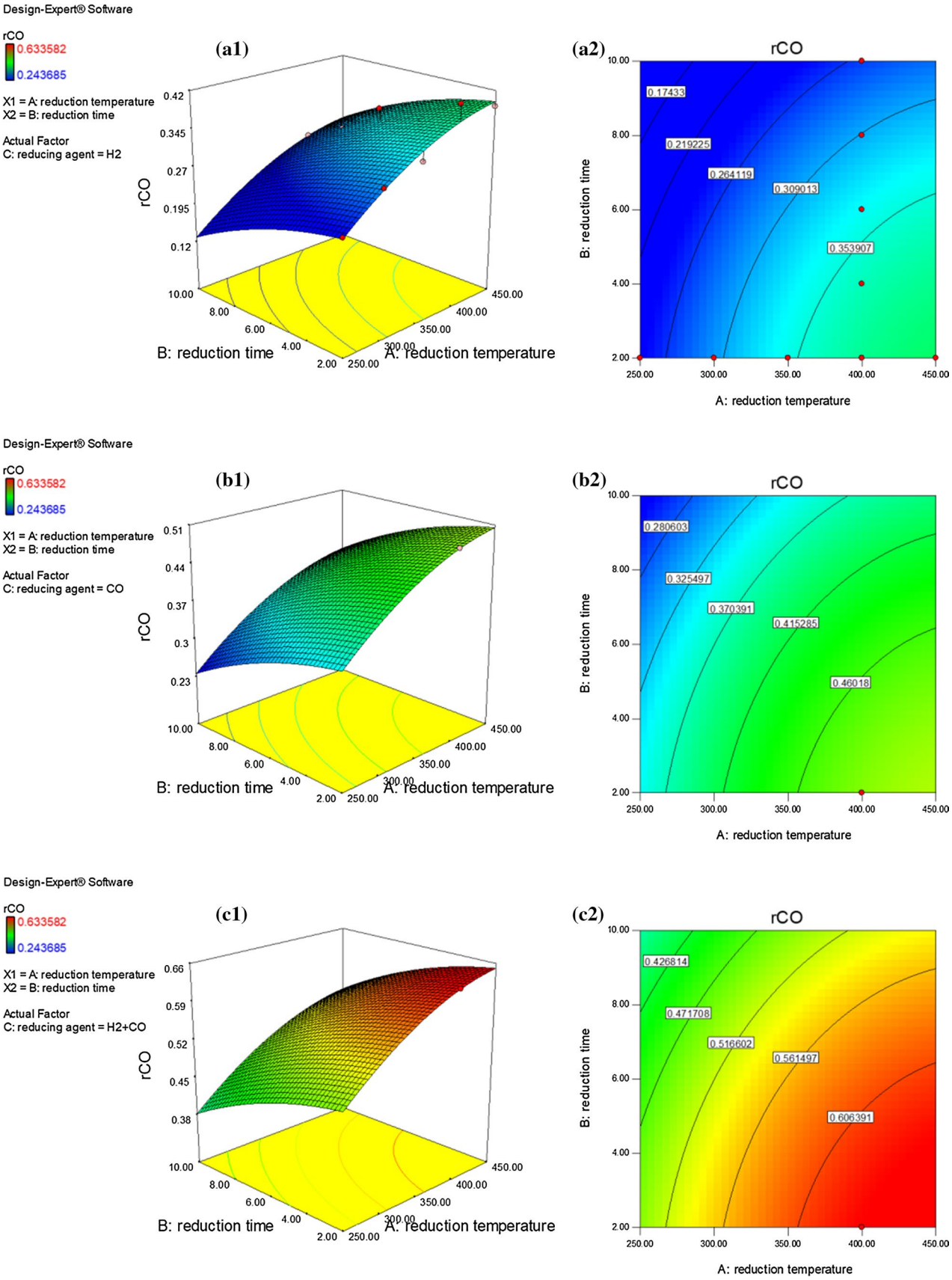
Design-Expert® Software
rCO
0.633582
0.243685
X1 = A: reduction temperature
X2 = B: reduction time
Actual Factor
C: reducing agent = H2
(a1)
rCO
0.42
0.345
0.27
0.195
0.12
B: reduction time
A: reduction temperature
(a2)
rCO
0.17433
0.219225
0.264119
0.309013
0.353907
B: reduction time
A: reduction temperature
Design-Expert® Software
rCO
0.633582
0.243685
X1 = A: reduction temperature
X2 = B: reduction time
Actual Factor
C: reducing agent = CO
(b1)
rCO
0.51
0.44
0.37
0.3
0.23
B: reduction time
A: reduction temperature
(b2)
rCO
0.280603
0.325497
0.370391
0.415285
0.46018
B: reduction time
A: reduction temperature
Design-Expert® Software
rCO
0.633582
0.243685
X1 = A: reduction temperature
X2 = B: reduction time
Actual Factor
C: reducing agent = H2+CO
(c1)
rCO
0.66
0.59
0.52
0.45
0.38
B: reduction time
A: reduction temperature
(c2)
rCO
0.426814
0.471708
0.516602
0.561497
0.606391
B: reduction time
A: reduction temperature

◂**Fig. 7.** 3D (1) and 2D (2) plots of the influences of the reduction temperature and time on CO consumption rate, at constant H_2 (**a**), CO (**b**), H_2+CO (**c**) reducing agents

The perturbation plot of CO consumption rate in terms of reaction parameters is shown in Fig. 6d. The steep slope of curve C demonstrates the CO consumption rate response is sensitive to it. This perturbation plot (Fig. 6d) proves that reaction pressure is the most significant factor for CO consumption rate.

After reviewing the model statistics and diagnostic plots, to study the effect of any two factors on CO consumption rate response, 3D and 2D plots were studied. Figure 7 shows curved surfaces, which represents the combined effect of reduction temperature and time on the CO consumption rate at each reducing agent. As can be seen, there are similar trends for all reducing agents (irrespective of the amount of CO consumption rate). In any fixed reducing agent, with an increase in reduction temperature and decrease in time, the CO consumption rate increased. The maximum CO consumption rate is happened at reducing agent of H_2+CO, reduction temperature of 450 °C and, reduction time of 2 h. While the minimum CO consumption rate belongs to the reducing agent of H_2, reduction temperature of 250 °C, and reduction time of 10 h.

The interaction effect of reaction temperature (A) and H_2/CO (B) at a constant pressure of 3 bar on CO consumption rate is shown in Fig. 8 (a1 and b1). As shown, with an increase in reaction temperature from 150 to 240 °C and H_2/CO from 1 to 4, the CO consumption rate increased and decreased, respectively. Also, it can be seen that the effect of the reaction temperature is more than H_2/CO, at a constant pressure of 3 bar. The binary effect of reaction temperature (A) and pressure (C) at fixed H_2/CO of 2.5 on the CO consumption rate is shown in Fig. 8 (a2 and b2). It was revealed that the CO consumption rate increased when the pressure changed from 1 to 5 bar as the reaction temperature increased. The steep slope of the pressure curve demonstrates that the reaction pressure is more effective than the reaction temperature. Also, with regard to Fig. 8 (a3 and b3), the pressure has more influence on the CO consumption rate rather than H_2/CO, too. Therefore, the obtained graphs illustrated that two parameters of P and T had considerable effects on the CO consumption rate of the Co–Ni/Al_2O_3 catalyst.

Catalyst characterization

To recognize the actual phases of the Co–Ni/Al_2O_3 catalyst in different steps of precursor, before and after the FTS reaction, the XRD technique was performed. The related XRD patterns are displayed in Fig. 9, which demonstrated that at different steps, different phases were made. As can be seen in Fig. 9a, the identified phases in the precursor catalyst consisted of hydrated metals nitrates (cobalt and nickel nitrate hydrate). While after heat treatment (Fig. 9b), the detected phases were Co_3O_4, CoO, NiO and, $NiCo_2O_4$ (oxidic phases). During the FTS, the catalyst was exposed to reactant gases such as H_2 and CO; therefore, the catalyst undergoes alterations. As can be observed in Fig. 9c, various carbidic and oxidic phases, including Co_3O_4, CoO, Co_3C, Ni_3C, and C were recognized in the catalyst after the test.

To investigate the morphological changes, the SEM images of the catalyst were evaluated. The SEM images disclosed alterations in the morphology of the precursor and catalyst after heat treatment and after the FTS. Regard to what is seen in Fig. 10a, there are large agglomerations with homogeneous and adhesive morphology in catalyst precursor. After the heat treatment (Fig. 10b), the size of these aggregates significantly has been reduced, and a structure with higher porosity rather than the precursor has been obtained, which could be due to the formation of small crystallite of cobalt and nickel oxides. By comparison of SEM images of catalysts before and after the FTS (Fig. 10b and c), it could be observed that the catalyst after the test contains smaller particles. Since the reactor temperature was not too high (180 °C), the sintering phenomenon, and then increase in particle size has not occurred. The decrease in particle size could be attributed to the formation of carbidic phases. The presence of carbidic phases in catalyst after the test was proved by XRD patterns.

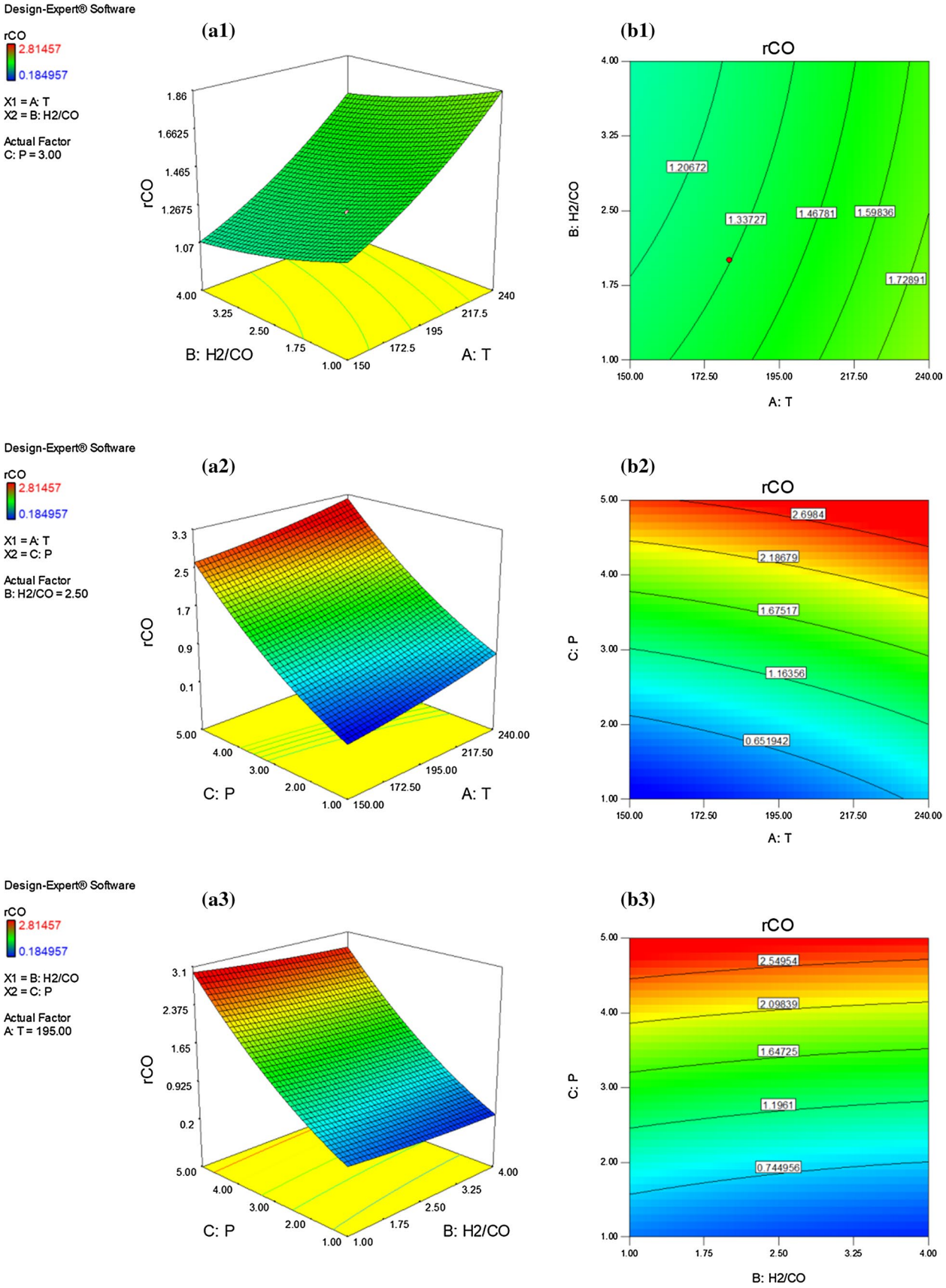

Fig. 8. 3D (**a**) and 2D (**b**) plots of the influences of the reaction conditions on CO consumption rate, at constant reaction pressure (**1**), H_2/CO (**2**), temperature (**3**)

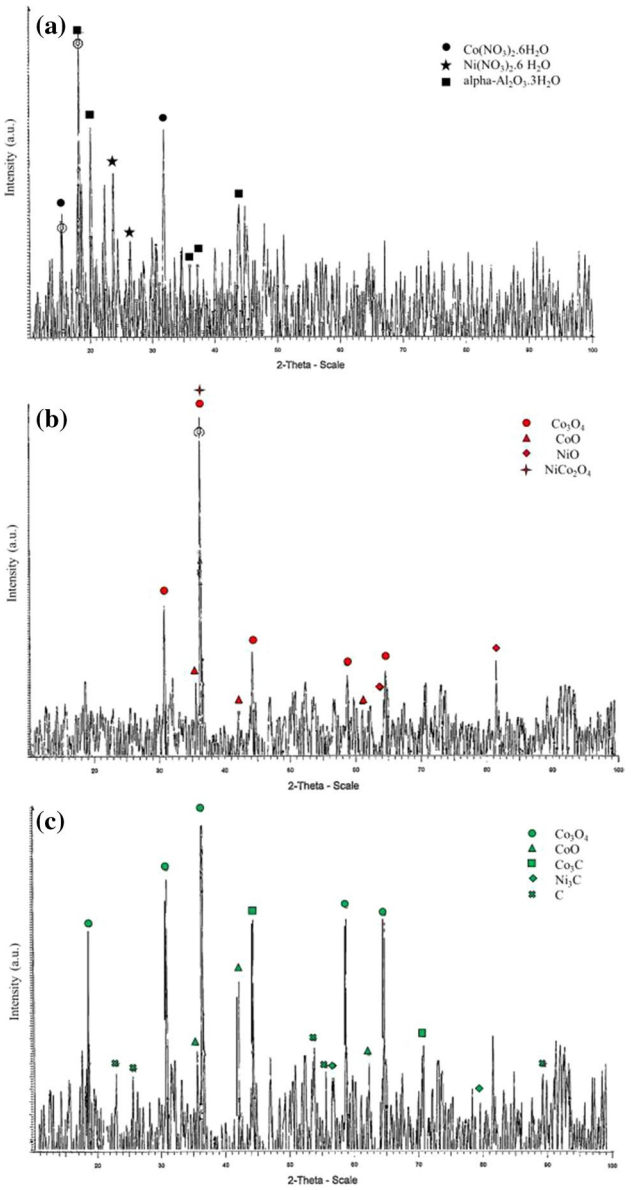

Fig. 9 XRD patterns of precursor (**a**), after heat treatment (**b**), and after the FTS (**c**) of Co–Ni/Al_2O_3 catalyst reduced by H_2 reducing gas

Conclusions

The catalytic performance of the Co–Ni/Al_2O_3 catalyst synthesized by the fusion method was evaluated in Fischer–Tropsch synthesis. Regard to the importance of modeling in FTS, in this study, the modeling of the effect of reduction and reaction parameters on CO consumption rate was performed. There are numerous studies which modeled the selectivity of FT products in terms of reaction conditions, but, to the best of our knowledge, there is no study about the modeling of the effect of reduction and reaction parameters on CO consumption rate. Therefore, in this study, in addition to evaluation of the reduction and reaction conditions on catalytic performance (catalyst activity and product selectivities), the modeling of CO consumption rate in terms of independent parameters of reduction and reaction conditions was performed, and the relationship between parameters and response was discussed. This goal was obtained using the RSM method. The obtained models demonstrated that the order of parameters influence on CO consumption rate is as below:

C (reducing agent) > A (reduction temperature) > B (reduction time) > A^2 > B^2.

C (reaction pressure) > A (reaction temperature) > B (H_2/CO) > C^2 > A^2 > B^2.

Therefore, reducing agent and reaction pressure have a considerable effect on the CO consumption rate. The 3D and 2D graphs demonstrated that maximum CO consumption rate occurred at reducing agent of $H_2 + CO$, reduction temperature of 450 °C and reduction time of 2 h. Also, it was revealed that the CO consumption rate increased when the pressure changed from 1 to 5 bar as the reaction temperature increased. The XRD and SEM of catalysts (precursor, before and after the FTS test) revealed that the operation condition has an obvious effect on the crystalline phases and morphology of the catalysts.

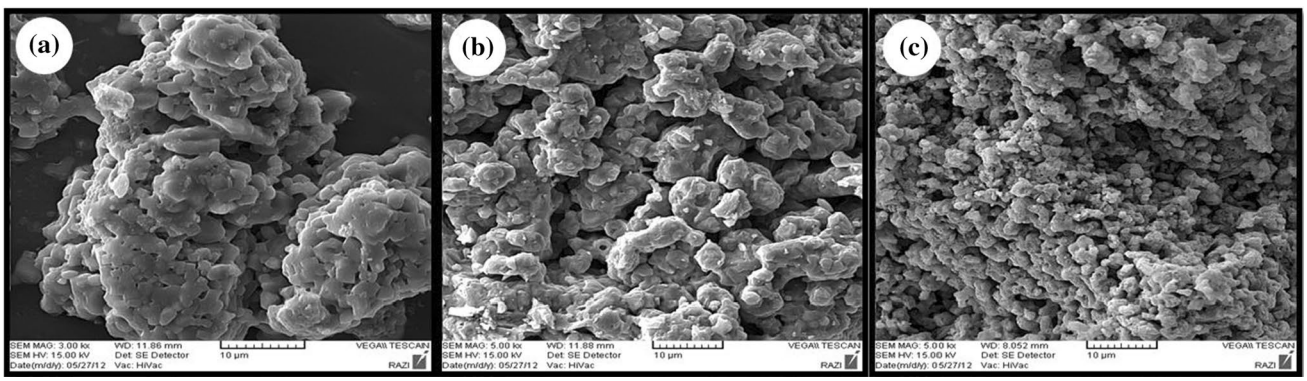

Fig. 10 The SEM images of precursor (**a**), catalysts before (**b**) and after the FTS (**c**)

Acknowledgements The authors acknowledge financial and instrumental support by the University of Sistan and Baluchestan.

Compliance with ethical standards

Conflict of interest None.

References

Abbasi M, Mirzaei AA, Atashi H (2019) Hydrothermal synthesis of Fe-Ni-Ce nano-structure catalyst for Fischer-Tropsch synthesis: Characterization and catalytic performance. J Alloy Compd 799:546–555

Akbari M, Mirzaei AA, Atashi H, Arsalanfar M (2018) Effect of microemulsion parameters on product selectivity of MgO-supported iron–cobalt–manganese–potassium nanocatalyst for Fischer-Tropsch synthesis using response surface methodology. J Taiwan Inst Chem Eng 91:396–404

Akbari M, Mirzaei AA, Atashi H (2019) Evaluation of reverse microemulsion parameters over the catalytic performance of promoted Fe–Co catalysts for the production of light olefins from syngas using box–behnken design. Catal Lett, pp 1–14.

Arsalanfar M, Mirzaei A, Bozorgzadeh H, Atashi H (2012) Effect of process conditions on the surface reaction rates and catalytic performance of MgO supported Fe–Co–Mn catalyst for CO hydrogenation. J Ind Eng Chem 18:2092–2102

Arsalanfar M, Akbari M, Mirzaei N, Abdouss M (2020) Light olefin production on the Co–Ni catalyst: calcination conditions, and modeling and optimization of the process conditions by a statistical method. New J Chem 44:7467–7483

Atashi H, Rezaeian F (2019) Modeling of Fischer-Tropsch synthesis product over an industrial fe-mn catalyst in a spinning basket reactor. Pet Sci Technol 37:1952–1959

Atashi H, Razmjooei S, Khorashadizadeh M, Shiva M, Tabrizi FF, Mousavi SAHS (2015) Effects of operating conditions on selectivity of Fe–Co–Mn/MgO at high temperature CO hydrogenation. J Taiwan Inst Chem Eng 54:83–90

Azizi HR, Mirzaei AA, Kaykhaii M, Mansouri M (2014) Fischer-Tropsch synthesis: studies effect of reduction variables on the performance of Fe–Ni–Co catalyst. J Nat Gas Sci Eng 18:484–491

Copperthwaite RG, Hutchings GJ, Van der Riet M, Woodhouse J (1987) Carbon monoxide hydrogenation using manganese oxide-based catalysts: Effect of operating conditions on alkene selectivity. Ind Eng Chem Res 26:869–874

Fazlollahi F, Sarkari M, Zare A, Mirzaei AA, Atashi H (2012) Development of a kinetic model for Fischer-Tropsch synthesis over Co/Ni/Al_2O_3 catalyst. J Ind Eng Chem 18:1223–1232

Feyzi M, Khodaei MM, Shahmoradi J (2012) Effect of preparation and operation conditions on the catalytic performance of cobalt-based catalysts for light olefins production. Fuel Process Technol 93:90–98

Jahangiri H, Bennett J, Mahjoubi P, Wilson K, Gu S (2014) A review of advanced catalyst development for Fischer-Tropsch synthesis of hydrocarbons from biomass derived syn-gas. Catal Sci Technol 4:2210–2229

Liu C, Chen Y, Zhao Y, Lyu S, Wei L, Li X, Zhang Y, Li J (2020a) Nano-ZSM-5-supported cobalt for the production of liquid fuel in Fischer-Tropsch synthesis: Effect of preparation method and reaction temperature. Fuel 263:116619

Liu Y, Chen Y, Yu H, Guan F, Hou Z, Cui D, Zhang Y (2020) Bimetallic Ni-Co catalysts for co-production of methane and liquid fuels from syngas, Catal. Today

Martinelli M, Karuturi SC, Garcia R, Watson CD, Shafer WD, Cronauer DC, Kropf AJ, Marshall CL, Jacobs G (2020) Substitution of Co with Ni in Co/Al_2O_3 Catalysts for Fischer-Tropsch Synthesis. Catalysts 10:334

Mirzaei A, Galavy M, Beigbabaei A, Eslamimanesh V (2007) Preparation and operating conditions for cobalt cerium oxide catalysts used in the conversion of synthesis gas into light olefins. J Iran Chem Soc 4:347–363

Mirzaei A, Rezazadeh E, Arsalanfar M, Abdouss M, Fatemi M, Sahebi M (2015) Study on the reaction mechanism and kinetics of CO hydrogenation on a fused Fe–Mn catalyst. RSC Adv 5:95287–95299

Moazami N, Wyszynski ML, Rahbar K, Tsolakis A, Mahmoudi H (2017) A comprehensive study of kinetics mechanism of Fischer-Tropsch synthesis over cobalt-based catalyst. Chem Eng Sci 171:32–60

Nisa MU, Chen Y, Li X, Li Z (2020) Highly efficient iron based MOFs mediated catalysts for Fischer-Tropsch synthesis: Effect of reduction atmosphere. J Taiwan Inst Chem Eng 107:44–53

Niu C, Xia M, Chen C, Ma Z, Jia L, Hou B, Li D (2020) Effect of process conditions on the product distribution of Fischer-Tropsch synthesis over an industrial cobalt-based catalyst using a fixed-bed reactor. Appl Catal A Gen, p 117630.

Ponec V (2001) Alloy catalysts: the concepts. Appl Catal A Gen 222:31–45

Rahmati M, Huang B, Mortensen MK Jr, Keyvanloo K, Fletcher TH, Woodfield BF, Hecker WC, Argyle MD (2018) Effect of different alumina supports on performance of cobalt Fischer-Tropsch catalysts. J Catal 359:92–100

Sari A, Zamani Y, Taheri SA (2009) Intrinsic kinetics of Fischer-Tropsch reactions over an industrial Co–Ru/γ-Al2O3 catalyst in slurry phase reactor. Fuel Process Technol 90:1305–1313

Sarkari M, Fazlollahi F, Ajamein H, Atashi H, Hecker WC, Baxter LL (2014) Catalytic performance of an iron-based catalyst in Fischer-Tropsch synthesis. Fuel Process Technol 127:163–170

Schulz H (2013) Principles of Fischer-Tropsch synthesis—Constraints on essential reactions ruling FT-selectivity. Catal Today 214:140–151

Sethuraman R, Bakhshi NN, Katikaneni SP, Idem RO (2001) Production of C4 hydrocarbons from Fischer-Tropsch synthesis in a follow bed reactor consisting of Co–Ni–ZrO2 and sulfated-ZrO2 catalyst beds. Fuel Process Technol 73:197–222

Shafer WD, Gnanamani MK, Graham UM, Yang J, Masuku CM, Jacobs G, Davis BH (2019) Fischer–Tropsch: Product selectivity–The fingerprint of synthetic fuels. Catalysts 9:259

Torres Galvis HM, de Jong KP (2013) Catalysts for production of lower olefins from synthesis gas: a review. ACS Catal 3: 2130–2149.

Tsakoumis NE, Rønning M, Borg Ø, Rytter E, Holmen A (2010) Deactivation of cobalt based Fischer-Tropsch catalysts: a review. Catal Today 154:162–182

Van Der Laan GP, Beenackers A (1999) Kinetics and selectivity of the Fischer-Tropsch synthesis: a literature review. Catal Rev Sci Eng 41:255–318

van Helden P, Prinsloo F, Van den Berg J-A, Xaba B, Erasmus W, Claeys M, van de Loosdrecht J (2020) Cobalt-nickel bimetallic Fischer-Tropsch catalysts: a combined theoretical and experimental approach. Catal Today 342:88–98

Weissman SA, Anderson NG (2014) Design of experiments (DoE) and process optimization. A review of recent publications. Org Process Res Dev 19: 1605–1633.

Yaghoobpour E, Zamani Y, Zarrinpashne S, Zamaniyan A (2020) Profound synergetic effect of metal oxide promoters and TiO2–SiO2 binary support in cobalt Fischer-Tropsch catalyst. J Chin Chem Soc 67:751–765

Zare A, Zare A, Shiva M, Mirzaei AA (2013) Effect of calcination and reaction conditions on the catalytic performance of Co–Ni/Al2O3 catalyst for CO hydrogenation. J Ind Eng Chem 19:1858–1868

Zarrin H, Sadeghi MT, Marvast MA (2009) Modeling and sensitivity analysis of a catalyst pellet with non-uniform activity distribution in Fischer-Tropsch synthesis. Int J Chem React Eng, 7